NOAA NESDIS
CENTER FOR SATELLITE APPLICATIONS AND RESEARCH

Vegetation Health Products (VHP) ALGORITHM THEORETICAL BASIS DOCUMENT

Version 1.0

VHP ALGORITHM THEORETICAL BASIS DOCUMENT VERSION 1.0

AUTHORS:

Felix Kogan (STAR)

Marco Vargas (STAR)

Hanjun Ding (OSPO)

Wei Guo (IMSG)

VHP ALGORITHM THEORETICAL BASIS DOCUMENT
VERSION HISTORY SUMMARY

Version	Description	Revised Sections	Date
1.0	New document adapted from SPSRB guidelines for VHP PDR	New Document	02/21/2011

TABLE OF CONTENTS

Page

LIST OF FIGURES 5

LIST OF TABLES 6

LIST OF ACRONYMS 7

ABSTRACT 9

1. INTRODUCTION 10
   1.1 PURPOSE OF THIS DOCUMENT 10
   1.2 WHO SHOULD USE THIS DOCUMENT 10
   1.3 INSIDE EACH SECTION 10
   1.4 REVISION HISTORY 11

2. VHP OVERVIEW 12
   2.1 OBJECTIVES OF VEGETATION HEALTH RETRIEVALS 12
   2.2 INSTRUMENT CHARACTERISTICS 12
   2.3 RETRIEVAL STRATEGY 13

3. ALGORITHM DESCRIPTION 14
   3.1 PROCESSING OUTLINE 14
   3.2 ALGORITHM INPUT 15
      3.2.1 AVHRR reflectance of visible and near infrared bands 15
      3.2.2 AVHRR Brightness Temperature 16
      3.2.3 Ancillary Data 16
   3.3 THEORETICAL DESCRIPTION OF RETRIEVAL VHP METHOD 18
   3.4 ALGORITHM OUTPUT 28
   3.5 PERFORMANCE ESTIMATES 28
      3.5.1 Test Data Sets 28

3.5.2 Sensor Radiometric Noise Effects 28
3.5.3 Sensor Radiometric Calibration Effects 30
3.5.4 Sensor Spectral Error Effects 31
3.6 PRACTICAL CONSIDERATIONS 33
3.6.1 Numerical Computation Considerations..... 33
3.6.2 Programming and Procedural Considerations 33
3.6.3 Quality Assessment and Diagnostics..... 33
3.6.4 Exception Handling..... 33
3.7 SAMPLE RESULTS 33
3.8 VALIDATION EFFORTS..... 34
4. ASSUMPTIONS AND LIMITATIONS 38
4.1 ASSUMPTIONS 38
4.2 LIMITATIONS 38
5. RISKS AND RISK REDUCTION EFFORTS 39
5.1 FAILURE OF AVHRR SENSOR ON NOAA SERIES SATELLITE. 39
5.2 AVHRR UNAVAILABILITY 39
6. LIST OF REFERENCES 40

LIST OF FIGURES

Page

Figure 1. Flow chart of VHP system 15

Figure 2. Land Cover Map Used by the VHP Algorithm 17

Figure 3. Dynamics of correlation coefficient between end-of-season MG corn yield departure from trend and spatial-average VCI during corn silking (critical period) 24

Figure 4. Example result of smoothing on time series of NDVI 26

Figure 5. Processed mean NDVI (left) and BT (right) for three global latitude bands..... 26

Figure 6. Dynamics of Vegetation health indices during the 2009 spring drought in southern Texas 27

Figure 7. Sensitivity of NDVI to noise of visible band 29

Figure 8. Sensitivity of NDVI to Change of Reflectance 30

Figure 9. Impact of calibration on NDVI..... 31

Figure 10. Response function of VIS and NIR bands for NOAA satellites..... 32

Figure 11. NDVI values calculated by 6S model from various NOAA satellites..... 32

Figure 12. Vegetation Health maps produced by the VHP algorithm 34

Figure 13. NDVI time series from GVPS, GIMMS and MODIS data sets..... 35

Figure 14. Time series of NDVI from AVHRR retrievals and NDVI from MODIS..... 36

Figure 15. Time series of NDVI from AVHRR retrievals and NDVI from MODIS..... 37

LIST OF TABLES

Page

Table 1. Summary of AVHRR/3 Spectral Channel Characteristics 13

LIST OF ACRONYMS

6S	Second Simulation of a Satellite Signal in the Solar Spectrum
ABI	Advanced Baseline Imager
ATBD	Algorithm Theoretical Basis Document
AVHRR	Advanced Very High Resolution Radiometer
BT	Brightness Temperature
EDF	Empirical Distribution Function
EPL	Enterprise Product Lifecycle
EUMETSAT	European Organization for the Exploitation of Meteorological Satellites
GAC	Global Area Coverage
GIMMS	Global Inventory Modeling and Mapping Studies
GLCC	Global Land Cover Characteristics
GVI	Global Vegetation Index
GVI-x	Global Vegetation Index of Extended Version
GVPS	Global Vegetation Product System
HDF	Hierarchical Data Format
IGBP	International Geosphere-Biosphere Programme
IMSG	I. M. Systems Group
IR	Infrared
km	kilometer
MB	Mega Byte
MCR	Multi Channel Retrieval
MetOp	Meteorological Operational satellite
MG	Minas Gerais
μm	micron
MODIS	Moderate Resolution Imaging Spectroradiometer
MSG	Meteosat Second Generation
MVC	Maximum Value Compositing
NASA	National Aeronautics and Space Administration
NCEP	National Center for Environmental Prediction
NDVI	Normalized Difference Vegetation Index
NESDIS	National Environmental Satellite, Data, and Information Service
NetCDF	Network Common Data Form
NIR	Near Infrared
NOAA	National Oceanic and Atmospheric Administration

OSPO	Office of Satellite and Product Operations
PDR	Preliminary Design Review
PNG	Portable Network Graphics
QA	Quality Assurance
SEVIRI	Spinning Enhanced Visible and Infrared Imager
SPSRB	Satellite Products and Services Review Board
STAR	Center for Satellite Applications and Research
TCI	Thermal Condition Index
TIFF	Tagged Image File Format
USGS	United States Geological Survey
VCI	Vegetation Condition Index
VF	Vegetation Fraction
VHI	Vegetation Health Index
VH	Vegetation Health
VHP	Vegetation Health Products
VIIRS	Visible/Infrared Imager Radiometer Suite
VIS	Visible channel

ABSTRACT

This document is the Algorithm Theoretical Basis Document (ATBD) for the Vegetation Health Operational Product System developed by the NOAA/NESDIS Center for Satellite Applications and Research (STAR). The main function of the VHP is to produce surface vegetation health indices from data from the Advanced Very High Resolution Radiometer (AVHRR) onboard NOAA polar-orbiting satellites, for applications in numerical weather and seasonal climate prediction models at the National Centers for Environmental Prediction (NCEP). The retrieval algorithm used in VHP is the Multi Channel Retrieval (MCR) algorithm using visible (VIS: 0.58–0.68 μm), near-infrared (NIR: 0.72–1.1 μm) and thermal (IR: 10.3–11.3 μm) bands. This document describes the details of the algorithm. To meet the data needs of NCEP and other potential users, the VHP was designed as a global weekly composite product. Details of these products are presented in Sections 2 and 3 of this document.

1. INTRODUCTION

NOAA has developed a new data set entitled the Vegetation Health Product (VHP). The VHP has advantages over other long-term global data sets (GIMMS, Pathfinder), being the longest (30-year), having the highest spatial resolution (4-km), containing, in addition to NDVI, data and products from infrared channels, originally observed reflectance and emission, many indices with suppressed noise, biophysical climatology and more importantly, products used for monitoring the environmental and socioeconomic activities (Kogan 1995, 1997). The algorithm was developed by scientists and developers of STAR VHP team led by Dr. Felix Kogan. The Office of Satellite and Product Operations (OSPO) will be responsible for data storage, accessibility and dissemination.

1.1 Purpose of This Document

The purpose of this document is to describe the VHP algorithm in detail for the STAR EPL Preliminary Design Review (PDR).

1.2 Who Should Use This Document

The intended users of this document include customers, STAR EPL PDR reviewers, VHP data users and VHP processing system operators.

1.3 Inside Each Section

This document contains the following sections:

Section 1.0 - Introduction. Section 1 provides the purpose, intended users, and revision history of the ATBD.

Section 2.0 - VHP System Overview. Section 2 describes the products generated by the algorithm and the characteristics of the instruments that supply inputs to the algorithm.

Section 3.0 - Algorithm Description. Section 3 describes the algorithm, including a processing overview, input data, physical description, mathematical description, algorithm output, performance estimates, practical considerations, and validation.

Section 4.0 - Assumptions and Limitations. Section 4 states assumptions that were made in determining that the software system architecture as designed will meet the requirements, and states limitations that may impact on the system's ability to meet requirements.

Section 5.0 - Risks and Risk Reduction Efforts. Section 5 describes algorithm risks and actions planned to reduce the risks,

Section 6.0 - List of References. Section 6 provides a list of references cited in the document.

1.4 Revision History

This is the original version (Version 1) of this document, dated February 2011. It has been produced for the VHP Preliminary Design Review (PDR). Updates will be incorporated into this document as the project progresses.

2. VHP OVERVIEW

2.1 Objectives of Vegetation Health Retrievals

The Vegetation Health Product (VHP) system is to meet the user request from NOAA-NCEP, numbered as #0911-0021 in the NESDIS Satellite Products and Services Review Board (SPSRB) Request Tracking System.

One of the most important long-term (30-year) satellite-based data records characterizing land surface, air temperature near the ground and climate was created from the Advanced Very High Resolution Radiometer (AVHRR) flown on the National Oceanic and Atmospheric Administration (NOAA) polar-orbiting satellites. Several global data sets have been developed from the AVHRR records since the early 1980s. They were the NOAA's Global Vegetation Index (GVI and GVI-2), National Aeronautics and Space Administration (NASA)'s Pathfinder and GIMMS (Tarpley et al 1984, James and Kalluri 1994, Kidwell 1997, Tucker et al 2004). These datasets focused only on the Normalized Difference Vegetation Index (NDVI), ignoring infrared measurements, which are very useful for monitoring land, climate and socioeconomics. Therefore, NOAA developed a new dataset entitled the Global Vegetation Health Product. The VHP has advantages over other long-term global data sets, being the longest (30-year), having the highest spatial resolution (4-km), containing, in addition to NDVI, data and products from infrared channels, originally observed reflectance and emission, many indices with suppressed noise, biophysical climatology and more importantly, products used for monitoring environmental and socioeconomic activities (Kogan 1995, 1997).

2.2 Instrument Characteristics

VHP requires the Normalized Difference Vegetation Index (NDVI) data for estimating the vegetation moisture condition and Brightness Temperature (BT) from infrared bands for estimating the surface thermal condition. Both parameters can be acquired from the AVHRR onboard all NOAA polar-orbiting Satellites. NOAA-19 satellite is currently the operational primary satellite for NOAA weather monitoring.

The AVHRR is a six channel scanning radiometer providing three solar channels in the visible-near infrared region and three thermal infrared channels (Table 1). More information on AVHRR is provided at
http://www.ncdc.noaa.gov/oa/pod-guide/ncdc/docs/klm/html/c7/sec7-1.htm

Table 1. Summary of AVHRR/3 Spectral Channel Characteristics

Parameter	Ch. 1	Ch. 2	Ch. 3A	Ch. 3B	Ch. 4	Ch. 5
Spectral Range (μm)	0.58-0.68	.725-1.1	1.58-1.64	3.55-3.93	10.3-11.3	11.5-12.5
Resolution (km) *	1.09	1.09	1.09	1.09	1.09	1.09

* VHP algorithm uses the AVHRR Global Area Coverage (GAC) data, which is at 4 km resolution

NDVI is basically a calculation of AVHRR channels 1 (RED) and 2 (NIR) using the equation:

$$NDVI = \frac{\rho_{NIR} - \rho_{RED}}{\rho_{NIR} + \rho_{RED}} \tag{2.1}$$

Brightness temperature from AVHRR channel 4 is used to characterize the surface thermal condition.

2.3 Retrieval Strategy

The basic retrieval strategy of the VHP system is to produce NDVI and Brightness Temperature from AVHRR observations and then compare them against their multiple year climatology. The VHP derived products are the Vegetation Condition Index (VCI), Temperature Condition Index (TCI) and Vegetation Health Index (VHI) which will be described in section 3 of this document.

3. ALGORITHM DESCRIPTION

3.1 Processing Outline

The VHP system generates weekly Vegetation Condition Index (VCI), Temperature Condition Index (TCI) and Vegetation Health Index (VHI) through the following steps:

Step 1: AVHRR daily maps are created by projecting AVHRR Global Area Coverage (GAC) observations from channels 1, 2, 4, and 5 into geographic grid (plate carree projection). Corresponding solar and satellite geometry angles are also saved.

Step 2: Weekly composite is created by selecting the pixels with maximum NDVI value from 7 AVHRR daily maps. Here, NDVI is calculated based on pre-launch calibration.

Step 3: From weekly composite, raw NDVI is calculated from AVHRR channels 1 and 2 after applying the most recent updated post-launch calibration. NDVI is adjusted using the Empirical Distribution Function (EDF) statistical technique. Brightness temperature (BT) is also calculated from AVHRR channel 4 after applying the non-linear correction.

Step 4: Noise from cloud contamination is further reduced by applying a digital smoothing filter on NDVI and BT.

Step 5: Climatology of NDVI and Brightness Temperature is calculated/updated from the multi-year smoothed NDVI and Brightness Temperature. Climatology variables include maximum, minimum, mean and standard deviation for NDVI and Brightness temperature respectively on a pixel by pixel basis.

Step 6: Vegetation Condition Index (VCI) is calculated by comparing the smoothed NDVI against the climatology (maximum and minimum) of NDVI for the corresponding week. Similarly, Thermal Condition Index (TCI) is calculated by comparing the smoothed BT against the climatology of BT. Vegetation Health (VH) is a combination of VCI and TCI.

The algorithm processing flow is shown in Figure 1.

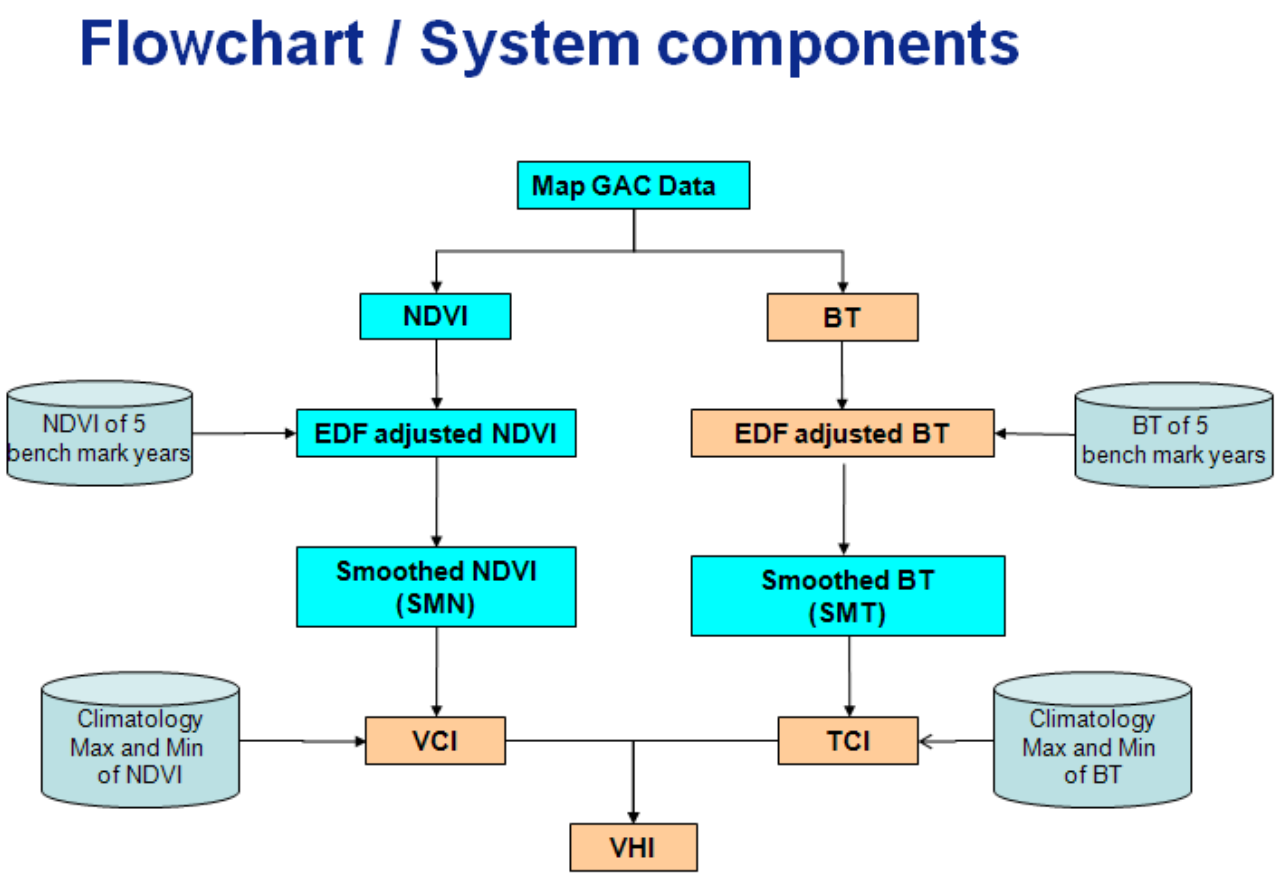

Figure 1. Flow chart of VHP system

3.2 Algorithm Input

3.2.1 AVHRR reflectance of visible and near infrared bands

AVHRR reflectance of visible and near infrared bands data are calculated from AVHRR GAC Level 1b radiance counts of visible (VIS, 0.58–0.68 µm), and near infrared (NIR, 0.725 – 1.1 µm) bands by applying pre-launch and post-launch calibration. The VHP algorithm uses the reflectance of these bands to calculate NDVI and moisture condition. AVHRR GAC data can be obtained through the Diamond or Emerald server.

Details on GAC data are available at http://www2.ncdc.noaa.gov/docs/podug/html/c3/sec3-1.htm

3.2.2 AVHRR Brightness Temperature

AVHRR brightness temperature data are from AVHRR GAC Level 1b calibrated brightness temperatures. The VHP algorithm uses brightness temperatures of AVHRR channel 4 (10.3–11.3 µm) to estimate thermal condition of land surface.

3.2.3 Ancillary Data

The ancillary data for the VHP algorithm include land cover map and NDVI climatology map.

3.2.3.1 USGS Land sea mask Map

It is USGS land sea mask in lat-lon grid with columns = 43200 and rows=21600, resolution 30 seconds. It covers full surface of the earth, latitude:[-90S to 90N], longitude: [-180,180]. The first pixel is at [-180,90N].

- landseamaskll.img 911MB,
  original raster image 43200x21600, 1 byte per pixel.
  This file was obtained from Dr. Aleksandar Jelenak.

- landseamaskll.img.bit 113MB,
  The binary data of bit map converted for above raster image. 1 bit per pixel.

- landseamaskll.bit.hdf 3MB.
  the HDF file contains the above bit map. 1 bit per pixel. The small file size is due to the compression feature of HDF. This file will be used as input when making daily and weekly composite maps.

3.2.3.2 Land Cover Map

The global land cover map is needed in this algorithm to correctly set the Quality Assessment (QA) for areas where the Vegetation Health retrieval capability of the VHP algorithm is weak, such as desert area. The International Geosphere-Biosphere Programme (IGBP) Land Cover map, i.e. Global Land Cover Characteristics Data Base (GLCC) was used. This clutter model provides global coverage at a 30 arc second

resolution using 17 clutter categories. Details are available at http://edc2.usgs.gov/glcc/ . The database consists of a single file - gigbp2_0ll.img (933,120,000 bytes). This file can be downloaded in a zipped format from http://edcftp.cr.usgs.gov/pub/data/glcc/globe/latlon/gigbp2_0ll.img.gz.

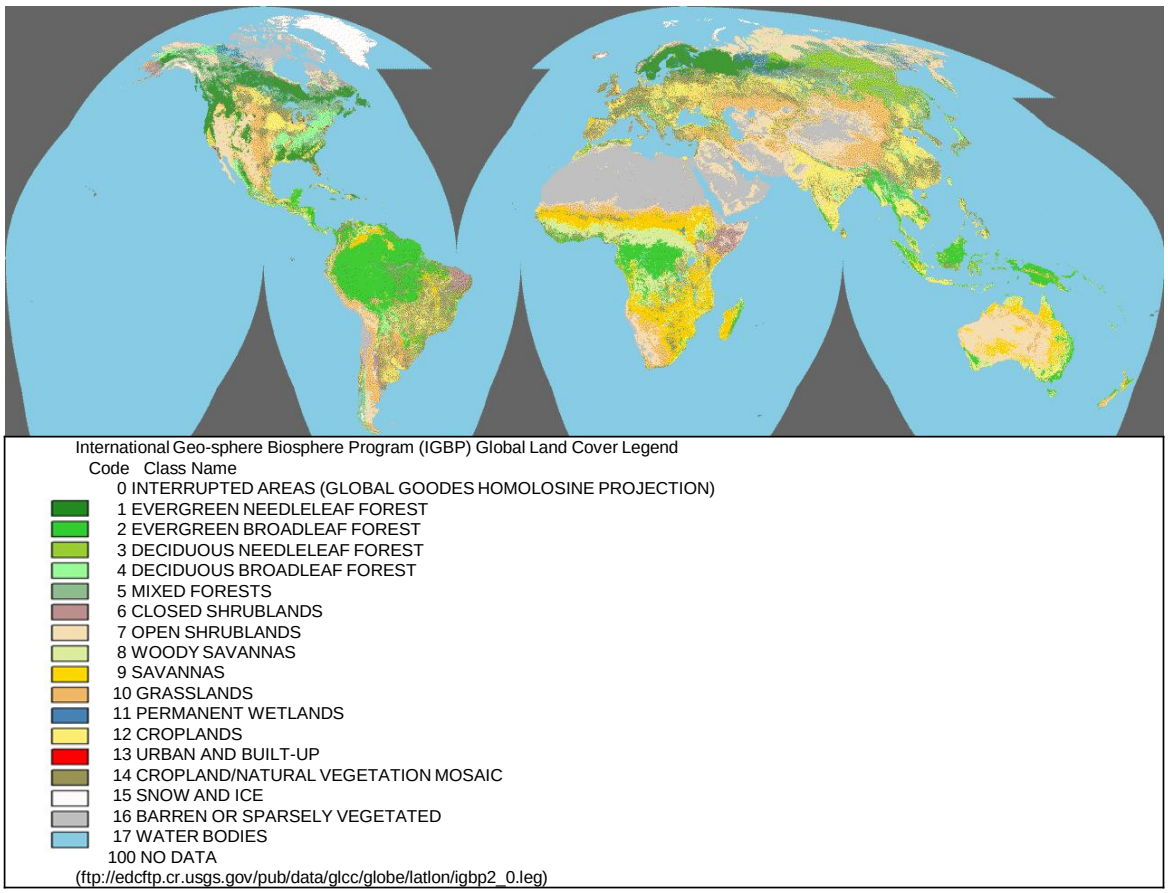

Figure 2. Land Cover Map Used by the VHP Algorithm

3.2.3.3 Climatology of AVHRR NDVI and Brightness Temperature

AVHRR NDVI and BT climatology maps were generated from 30 year smoothed weekly NDVI and BT.

There are 8 data fields: maximum, minimum, mean and standard deviation for NDVI and BT respectively. They are statistics based on smoothed NDVI and BT on a pixel by pixel basis.

3.2.3.4 Calibration parameters

Pre-launch and post-launch calibration parameters are provided in separate files. Those parameters help convert radiance counts of AVHRR VIS and NIR bands to reflectances.
When making daily and weekly composite maps, pre-launch calibration parameters were used. When calculating NDVI, both pre-launch calibration and optimized post-launch calibration are applied. In real-time (operational) situation, the most recent updated post-launch calibration are considered as “optimized post-launch calibration”.

3.3 Theoretical Description of Retrieval VHP Method

After noise removal, weather-driven differences in NDVI and BT between the years become apparent: lower NDVI and higher BT in dry years and opposite in normal and wet years. This principle of comparing NDVI and BT for a particular year with their dry-wet range calculated from 30-year observations was laid down in the VHP algorithm development. The absolute maximum and minimum of NDVI and BT during 1981-2005 were calculated for each of the 52 weeks and for each pixel. They were then used as the criteria to estimate the upper (favorable weather) and the lower (unfavorable weather) limits of the ecosystem resources. Further, for estimation of weather impacts on vegetation condition, NDVI and BT values for a particular time (one week or several weeks) were normalized relative to the absolute max/min interval. Following this procedure, NDVI and BT were rescaled based on equations (3.1-3.3). They were named the Vegetation Condition Index (VCI), Temperature Condition Index (TCI) and Vegetation Health Index (VHI) designed to characterize moisture (VCI), thermal (TCI) and total vegetation health (VHI) conditions in response to weather impacts

$$VCI=100*(NDVI-NDVImin)/(NDVImax-NDVImin) \quad (3.1)$$

$$TCI=100*(BTmax - BT)/(BTmax - BTmin) \quad (3.2)$$

$$VHI = a*VCI + (1- a)*TCI \quad (3.3)$$

where NDVI, NDVImax, and NDVImin (BT, BTmax, and BTmin) are the smoothed weekly NDVI (BT), their multi-year absolute maximum, and minimum, respectively. The VCI, TCI

and VHI approximate the weather component in NDVI, BT and their combination values. They fluctuate from 0 to 100, reflecting changes in vegetation conditions from extremely bad to optimal. The weighting factor (a) in equation 3.3 was determined by experience, currently, a=0.5).

VHP daily map

The VHP system algorithm starts from data extraction from the AVHRR GAC L1B file and collating the data onto a global VHP grid. This grid is based on the Plate Carree map projection. The global data spans from 75.024° (north edge) to -55.152° (south edge) in the latitudinal and from -180° (west) to 180° (east) in longitude directions. This processing supports nominal grid cell length of 4-km (3,616*10,000 grid elements).

VHP weekly composite

The VHP input includes the AVHRR observation, and geo-location information for each GAC Level 1B orbit. Daily data are aggregated to a seven-day period using a Maximum Value Compositing (MVC) method (saving the day which has the highest NDVI during the period). The compositing starts on the first day of a year and a period must have at least four days in the same year. The VHP weekly composite is a single file for each processing period containing metadata for each output variable, sensor and solar zenith angle, relative azimuth angle and ch1, ch2 counts and ch4, ch5 brightness temperature in a NetCDF file.

Calibration

One of the important steps in the primary data processing is radiometric calibration of visible channels 1 and 2. Visible channel calibration consists of generally two steps: pre-launch and post-launch calibration. Based on Kidwell (1995), the following pre-launch linear formula is applied to each of channels 1 and 2:

» $A = S*C + I$

where A = derived albedo for the channel, C = observed digital count for the channel, and the channel-specific parameters S and I are pre-determined.

Since the instrument output does not remain the same after launch, post-launch calibration is applied for NOAA-7 to 14 satellites, following Rao and Chen (1993, 1999):

» $R = S*(C - C_D)$

where R = derived TOA reflectance for the channel, C = observed digital count for the channel, the instrument-specific and channel-specific parameter S is pre-determined, and C_D is a pre-determined instrument-specific and channel-specific dark count).

For NOAA-16 through 19 a dual slope calibration method is applied:

» $R = S_L*C + I_L$; $(C < C_T)$

» $R = S_H*C + I_H$; $(C > C_T)$

where R = derived TOA reflectance for the channel, C = observed digital count for the channel, the instrument-specific and channel-specific parameters S_L, I_L, S_H, I_H are pre-determined, and C_T is an instrument-specific and channel-specific threshold count value that is also pre-determined (~ 500).

Thermal Correction

One of the important steps in the primary data processing is correction of thermal channel 4. This is an instrument-specific correction for NOAA-9, 11, and 14 only. Details will be provided in a future version of this ATBD.

Long- and Short-term Noise

Noise in AVHRR data creates fundamental constraints to the remote sensing of the Earth. The noise sources are physical, geometrical, mechanical, mapping, environmental, random etc; some of them long-term, some short-term and some both (Kogan *et al* 1996, Rao and Chen 1993, 1999, Cracknell 1997, Kidwell 1997). Clouds and other atmosphere constituents (aerosol, water vapor etc) obscure the land surface reducing NDVI considerably. In case of unusual events, such as sharp volcanic aerosol increase, NDVI can be depressed for a long time (Kogan et al., 1994). Changes in viewing and illumination geometry can lead to both an increase and decrease in NDVI depending on location, type of vegetation, position of sun and sensor. Satellite orbital drift, sensor degradation, and satellite change create long-term noise in NDVI data, especially after a satellite has been in service for more than three years.

A few techniques have been designed to detect and reduce some noise in AVHRR data such as cloud and aerosol-screening, bi-directional and radiative transfer models, pre- and post-launch calibration, geometry effects, sensor degradation and satellite orbital drift. Regardless of all these achievements, a complete physically based correction for all effects over various land surfaces, able to eliminate high, medium and low frequency noise, is not available. Unfortunately, NDVI and BT annual time series values experience large fluctuations (Kogan, 1995) introducing some errors when this data is used for monitoring purposes. Many of these fluctuations are associated with non-physical causes, such as method of data sampling and processing, satellite navigation and orientation, observation and communication errors, and other random noise. It is unlikely to develop corrections for this type of noise. Besides, if clouds are detected the data are discarded, leaving a gap on a map. This put additional constraint on AVHRR data utility.

In the development of VHP method and algorithm, major long- and short-term noise creating problems for satellite data interpretation and applications was removed from the data. They are:

(a) Satellite orbit and sensor degradation;

(b) Jumps between the satellites;

(c) Excessive stratospheric aerosols;

(d) Difference in Equator crossing time;

(e) Difference between AVHRR sensors;

(f) High frequency (short-term) noise;

(g) Random noise.

Some of the noise sources are interrelated, some have additive impact, some has either short- or long-term contribution and some provides a combined input. Visible channels are affected by all noise sources, while infrared mostly by short-term because they are calibrated on board.

Large satellite data distortion in the visible channels and NDVI occurs due to such long-term noise as satellite orbital drift, AVHRR sensor degradation and excessive stratospheric aerosols from volcanoes. The orbital drift and sensor degradation affected visible measurements on all space platforms; they normally start 2-3 years after a satellite was launched into space. NDVI reduction was observed on the data collected from NOAA-9 during 1987 and 1988, NOAA-11 (1993 and 1994) and NOAA-14 (1999 and 2000). In

addition, reflectance/emission measured from NOAA-11 were distorted due to elevated stratospheric aerosols during 1991-1993 resulted in NDVI reduction. The aerosol was built after eruption of Mt Pinatubo volcanoes in the Philippines in mid-June 1991. In a few weeks after eruption, the aerosols encircled the Earth with the major air flow and stayed in the area between 30-20º N and 20-25º S for nearly 1.5-2 years. As the result the NDVI in that area dropped almost in half during second part of 1991 through 1992 (Kogan *et al.* 1996, Vargas *et al.* 2009). Similarly, NDVI reduced in tropical latitudes in April 1982 for one-two years after eruption of El Chichon volcano in Mexico (Stowe *et al*. 1992).

Some difference between NDVI calculated from NOAA-16 and 18 satellites reflectance and from NOAA-14 and 11 existed during 2000-2010. This occurred because the AVHRR-3 instrument has slightly different characteristics than AVHRR-2. Specifically, the area under response function curve for the first two was 8-12% narrower than for the last two. As a result the NDVI from NOAA-16 and 18 turned out to be higher than for the previous satellites. Moreover, in addition to NDVI reduction for NOAA-7 and 9 due to stratospheric aerosol and severe orbit degradation, the magnitude of NDVI for the 1981-1988 period was 10-15% smaller than for the next two satellites because the time of the equator crossing for the first two satellites was almost one hour later. As a result of these problems and also orbit-degradation errors, large jumps in NDVI were observed between the end of previous and the beginning of the next satellites. The IR channels are also affected by stratospheric aerosol and orbit degradation (although less than the VIS) and must be corrected.

Finally, high frequency noise inside each year created by clouds, variable transparency of the atmosphere (water vapor, dust, chemicals etc), surface anisotropy, geometry of the sun and sensor, position of satellite, methods of data processing, random noise (including human errors) and long-term sources of noise distort considerably reflectance/emission of both NDVI and BT creating difficulties for satellite data application.

Noise removal

As it has been mentioned, quite often different sources of noise affect NDVI and BT either reducing their values (sensor degradation, orbital drift, equator crossing time, atmospheric attenuation, volcanic eruptions, etc) or increasing (spectral response function, off-nadir view, etc) or both depending on parameters (sensor type, surface anisotropy, forward/backscattering, sampling, random errors, etc). Moreover, quite often, several sources of noise affect the measured parameters at the same time and with different intensity. It is hard to develop individual procedure for each source of noise because it is unknown how to separate them (for example elevated stratospheric aerosol and sensor/orbit degradation). Therefore, the noise in VHP data is removed empirically by comparing satellite and in situ observations applying the methods of mathematical statistics plus validation.

Bias related to sensor degradation, satellite orbital drift, jumps in the indices while transitioning from one satellite to the next/previous and an elevated stratospheric aerosol load was removed by applying the Empirical Distribution Function (EDF) method (Crosby et. al. 1996). The EDF method is based on the assumption that for large areas, the NDVI reduction due to technical and external forces (orbital drift, volcanic eruptions, etc) is larger than the weather-related NDVI changes from year to year. An EDF is a cumulative distribution function that gives the probability that a random variable X is less than a given value x [$F(x) = Pr\{X < x\}$]. Following this assumption, large and stable changes in NDVI and BT can signal unexpected disturbances due to non-weather related causes discussed here. As a rule, sensor and satellite orbital degradation, jumps and aerosol reduce NDVI and BT. This negative effect can be reduced by adjusting the EDF of the affected years with a benchmark EDF from non-affected years. The benchmark EDF for NDVI and BT was statistically composited of data from five non-affected years: 1989, 1990, 1995, 1996, and 1997 (Vargas et al., 2009). The benchmark EDF for NDVI and BT was developed for each latitude line and week of the year. The normalization of the distorted data was performed for each pixel inside every latitude line and for each week. The thresholds (0.01 for NDVI and 2º C for BT) for the correction were selected based on data analysis.

The results of the EDF procedure were tested to verify that the method does not distort the data. In our earlier research it was shown that the AVHRR based vegetation health (VH) indices correlate strongly with crop yield in different parts of the world including Brazil (Salazar et al, 2007; Lui and Kogan, 2002). Therefore, corn yield data during 1985-1995 were collected from the aerosol affected Minas Gerais (MG) state of Brazil. For the major corn area of MG (46°W- 47°W, 16°S-17°S), the average spatial values of the NDVI-based Vegetation Condition Index (VCI) (Kogan, 1997) were calculated for each week of the

1985-1995 period (two datasets: aerosol affected and normalized). Then, end of season MG corn yield deviation from technological trend was correlated with weekly VCI of the 1985-1995 period.

Figure 3 displays test results. As seen, during silking, which is the critical period of corn development, correlation between corn yield deviation from 1985-1995 trend and weekly VCI for both data is increasing from near zero in the pre-silking time to 0.45 at the peak of the silking and drops to zero in post-silking time. The improved data show higher correlation than the aerosol distorted. Although the differences are not larger than 0.1 still this test confirms the utility of the normalization procedure.

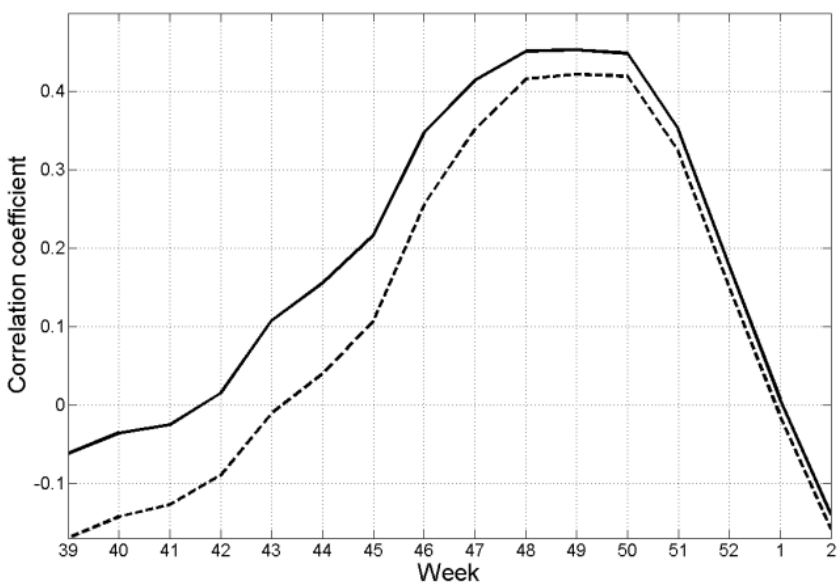

Figure 3. Dynamics of correlation coefficient between end-of-season MG corn yield departure from trend and spatial-average VCI during corn silking (critical period)

In Figure 3, the solid line is normalized NDVI, dashed line is aerosol-affected NDVI. A stable long-term bias between NDVI from NOAA-16 , 18 (2000-2010) and previous satellites due to response function differences was removed by calibrating the distorted NDVI against the NDVI measured by an on-ground radiometer during the growing season of 2002 over soybeans and corn at the experimental station of the University of Nebraska-Lincoln. During that period the fields' vegetation fraction (VF) changed from 10% at the beginning of the season to 90% at the end. The in situ NDVI was compared with the top-of-

canopy NDVI (obtained by running radiative transfer model) from AVHRR-3 sensor on NOAA-16. The comparison showed that NOAA-16 and later NOAA-18 and NOAA-19 NDVI must be reduced by 10%.

Another stable long-term bias, lower NDVI level for NOAA-7 and 9 (1981-1989) compared to the later satellites, was investigated. A ½ hour data collected from the Spinning Enhanced Visible and Infrared Imager (SEVIRI) on the Meteosat Second Generation (MSG) European satellites was used to investigate NDVI dynamics in relation to the local time of observations. The results indicated that the bias developed because for the earlier satellites, the equator crossing time was ½ to one and a half hours later than for the following satellites. SEVIRI's NDVI analysis for the year 2009 indicated that NDVI drops between 6 and 11% if observation local time moves from 13:00 pm to 14:30 pm. In order to correct this distortion the EDF method was used.

High frequency noise (clouds, aerosol, bi-directional reflectance, sun and sensor angles, human errors, other random noise) were removed from NDVI and BT by applying statistical methods. The vegetation-oriented method for a comprehensive noise reduction stems from a statistical approximation of the vegetation and temperature annual time series. The idea was to (a) single out the seasonal cycle; (b) suppress high frequency noise, and (c) enhance medium and low frequency variations related to large-scale and persistent weather fluctuations. This technique considers smoothing the weekly time series with a combination of a compound median filter and the least squares technique (Kogan et al. 1993). Numerous tests showed that this smoothing eliminated completely the high frequency outliers, including random, approximated accurately the annual NDVI and BT cycles, and, more importantly, singled out medium-to-low frequency weather-related fluctuations (valleys and hills in the NDVI and BT time series) during the annual cycle (Kogan, 1995). Figure 4 shows the effect of the smoothing filter on a time series of NDVI.

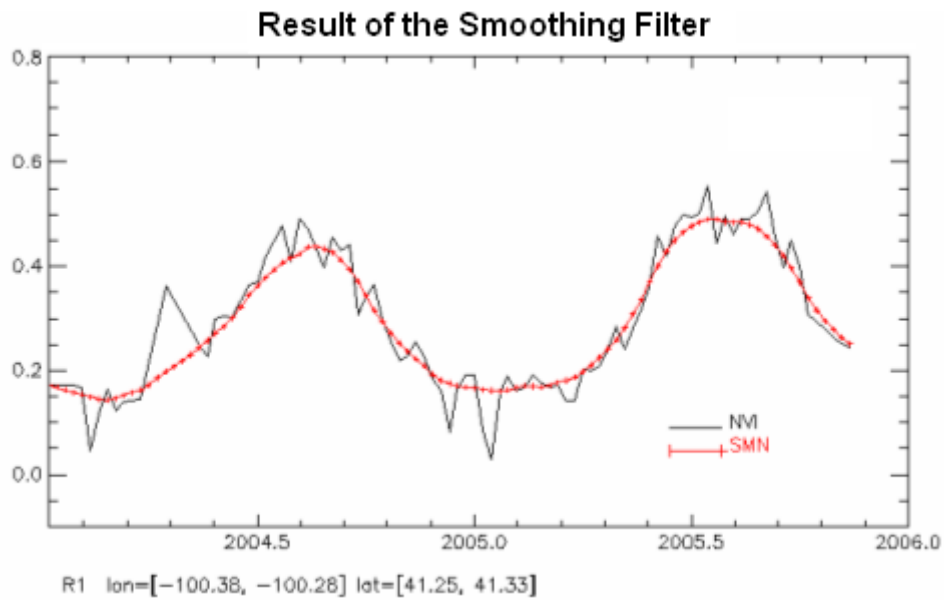

Figure 4. Example result of smoothing on time series of NDVI

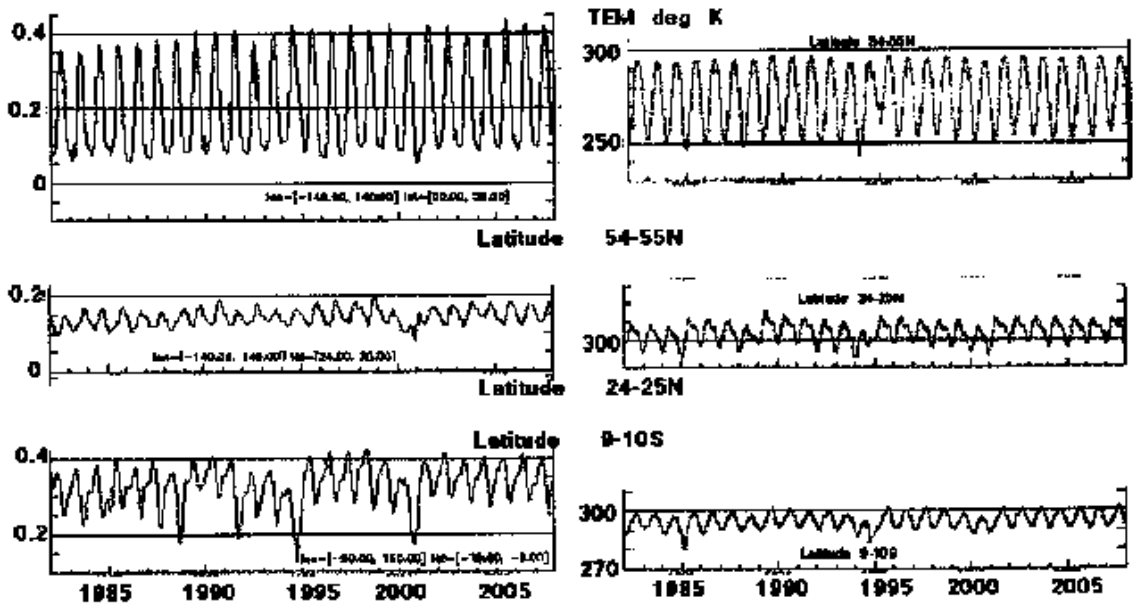

Figure 5. Processed mean NDVI (left) and BT (right) for three global latitude bands

Figure 5 shows time series of completely processed no noise NDVI averaged over three 1.0º latitudinal circles. Each diagram covers several ecosystems: broadleaf forest (54.5º-55ºN), mostly desert with some contribution from Southeast Asia forest (24.5º-25ºN) and mostly tropical forest (5.0º-5.5ºS). As seen, the time series show neither long-term trend nor short-period (5-10 years) trends. There are not any jumps between the satellites (1985-86, 1988-89, 1994-95), no NDVI reduction due to satellite orbit, sensor degradation and excessive stratospheric aerosols (1982-1984 and 1991-1994); (d) no difference due to Equator crossing time; (e) no difference due to AVHRR sensors changes; and (f) no high frequency and random noise are observed.

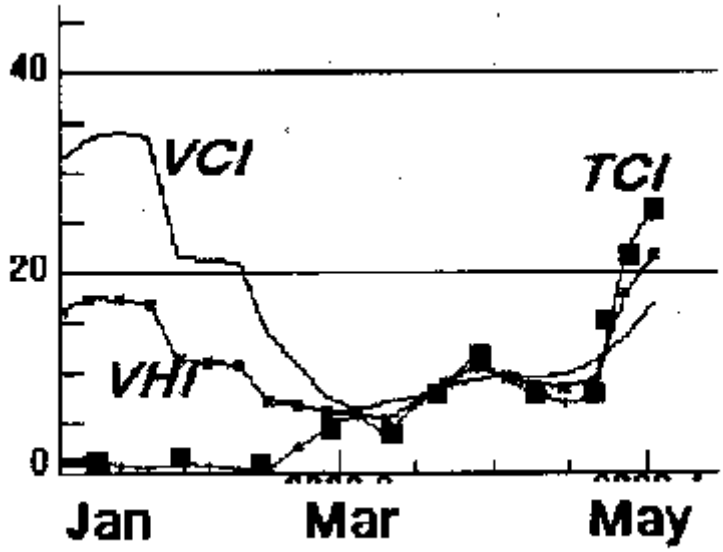

Figure 6. Dynamics of Vegetation health indices during the 2009 spring drought in southern Texas

An example of VH assessment and analysis of the 2009 spring drought in southern Texas (for a box with longitude 98.0-97.7º W, latitude 28.0-28.3º N from NOAA-18 satellite) is shown in Figure 6. As seen, all indices show drought (below 40) from January 2009. The unfavorable conditions developed due to extremely high temperatures (TCI close to 0), which continued through the entire spring (almost four months). As a result of the extreme

heat, VCI (moisture index), which indicated mild (30-40) drought in January deteriorated quickly reaching extreme drought level of 5-10 during March and April. Since both VCI and TCI showed extreme drought conditions the total vegetation health conditions were extremely unfavorable. In May, drought recovery started, because the temperature cooled off.

3.4 Algorithm Output

The outputs of Vegetation Health Product (VHP) system include:

(1) Three vegetation indices (VCI/TCI/VHI) on geographic projection grid with 4km resolution stored in a NetCDF file.

(2) Images of vegetation indices and other further derived indices (for example, drought index, and fire risk index) in 16km resolution, stored in PNG file format.

(3) Vegetation indices data in Geo-TIFF

3.5 Performance Estimates

By using the climatology data and comprehensive digital filters, the VHP system can produce vegetation health indices for the “global” area (from 55º S to 75º N) except for desert, snow (or extremely cold) area for each week.

3.5.1 Test Data Sets

The GVI-x dataset was used as test data set. VHP was run for NOAA 7,9,11,14,16,17,18 and 19. AVHRR daily maps, weekly composites and derived vegetation indices were produced for the period from 1981 to 2010. VHP products were compared with GVI-x dataset which is research prototype for VHP system.

3.5.2 Sensor Radiometric Noise Effects

Sensitivity study show if noise added = 0.3% on visible band (corresponding to signal/noise = 29.6 for low reflectance of 5%), NDVI change will be 3 % (NDVI>0.7) to 6% (NDVI = 0.1). Results are shown in Figure 7.

NDVI changes with noise in Visible band
Noise of Albedo added = 0.3

(for low Reflectance 5%, noise 0.3% corresponding to signal/noise =29.6)

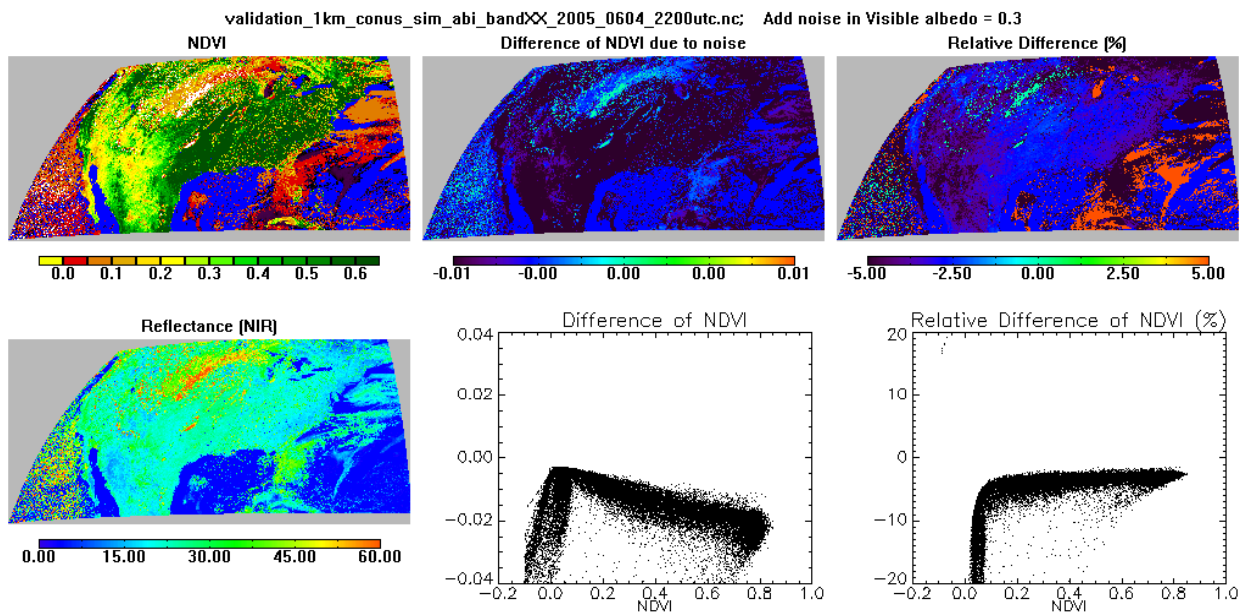

The input reflectance of visible and NIR bands are ABI simulated 1km data at ABI band 2 and 3.

Please note: the statistics includes data with the cloud.

Figure 7. Sensitivity of NDVI to noise of visible band

The Sensitivity of NDVI to Change of Reflectance was investigated by applying delta-R to reflectance of CH1 or CH2. The results (Figure 8) show NDVI is more sensitive to variation for target with low reflectance than high reflectance.

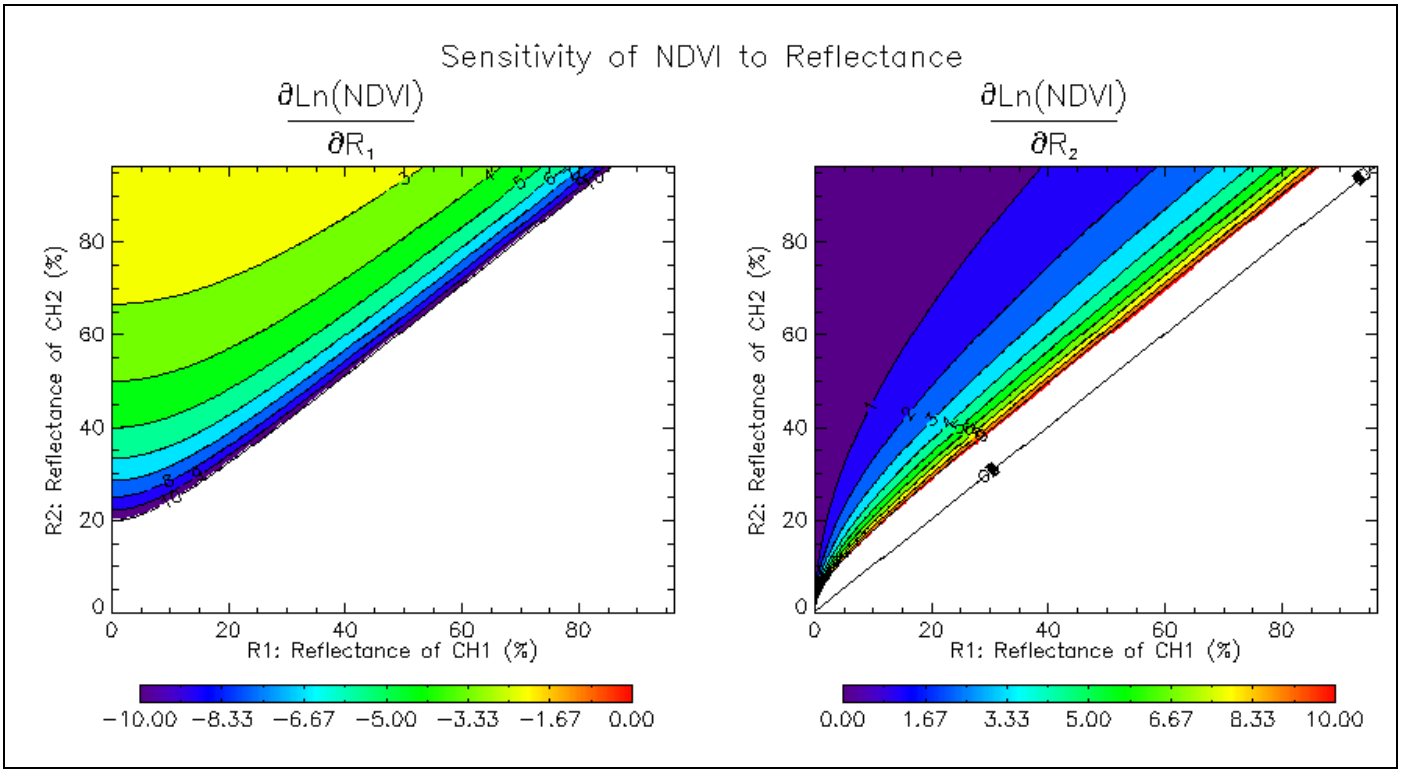

Figure 8. Sensitivity of NDVI to Change of Reflectance

3.5.3 Sensor Radiometric Calibration Effects

For a given satellite, calibration parameters were calculated and updated every month. The calibration parameters obtained in September, October and November of 2005 were applied to VHI composite of the same week, and it was found that the NDVI with smaller values changed more than NDVI with higher values as seen if Figure 9. In other word, due to the non-linear feature, calibration affects pixels with low NDVI more than pixels with high NDVI.

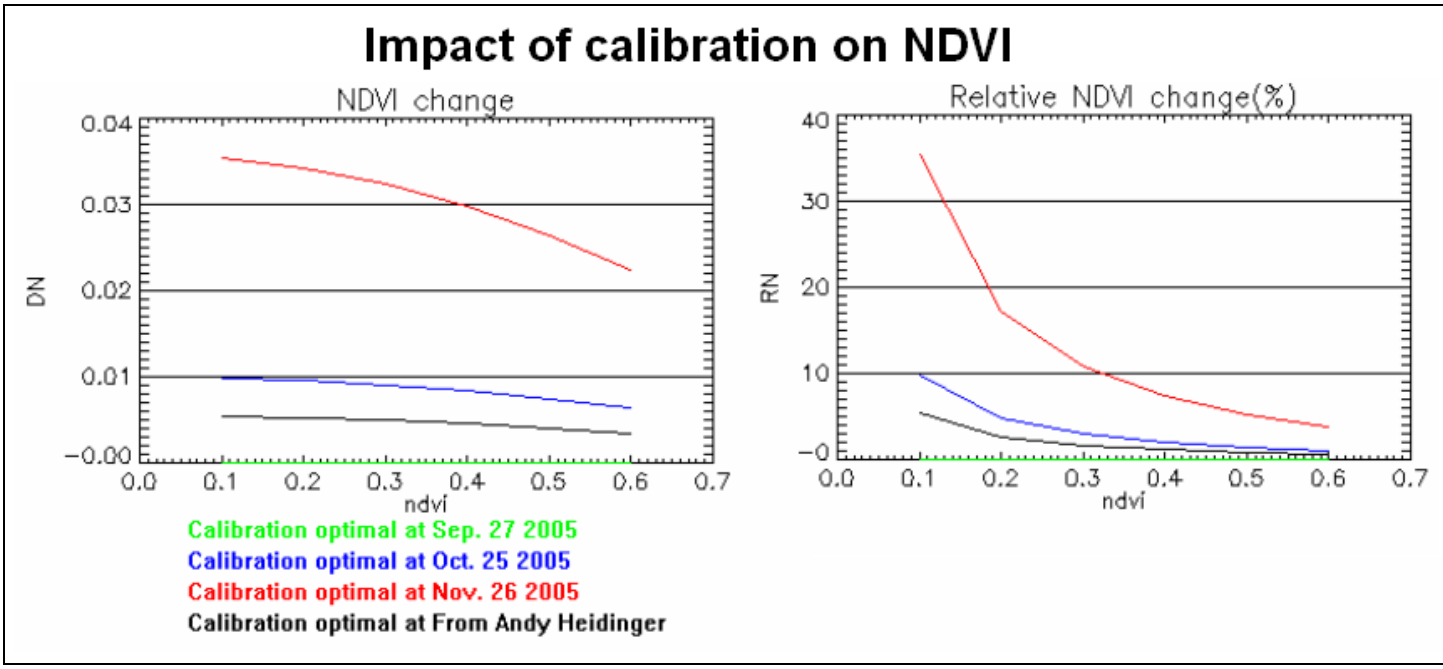

Figure 9. Impact of calibration on NDVI

3.5.4 Sensor Spectral Error Effects

The AVHRR instruments were designed in different decades and subject to significant improvement during the last 30 years. Figure 10 shows the spectral response functions of VIS and NIR bands for NOAA satellites (NOAA 7 to 19, afternoon satellites only). The VIS channels of the third generation AVHRR instruments (onboard NOAA 15,16,17,18 and 19) have narrower band width than the first and second generation of AVHRR instruments. Using 6S radiative transfer code (**S**econd **S**imulation of a **S**atellite **S**ignal in the **S**olar **S**pectrum), we calculated the NDVI values for 4 different types of surface for which we knew the reflectance at each wavelength (Figure 11). The result shows that for dense vegetation, NDVI observed by the third generation of AVHRR is much higher than the previous satellite. This result is identical to what we observed by real satellite data.

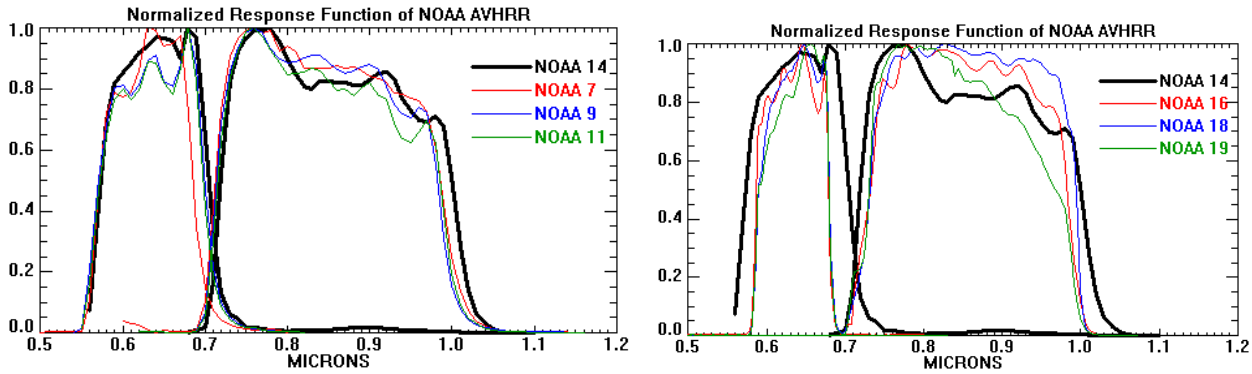

Figure 10. Response function of VIS and NIR bands for NOAA satellites.

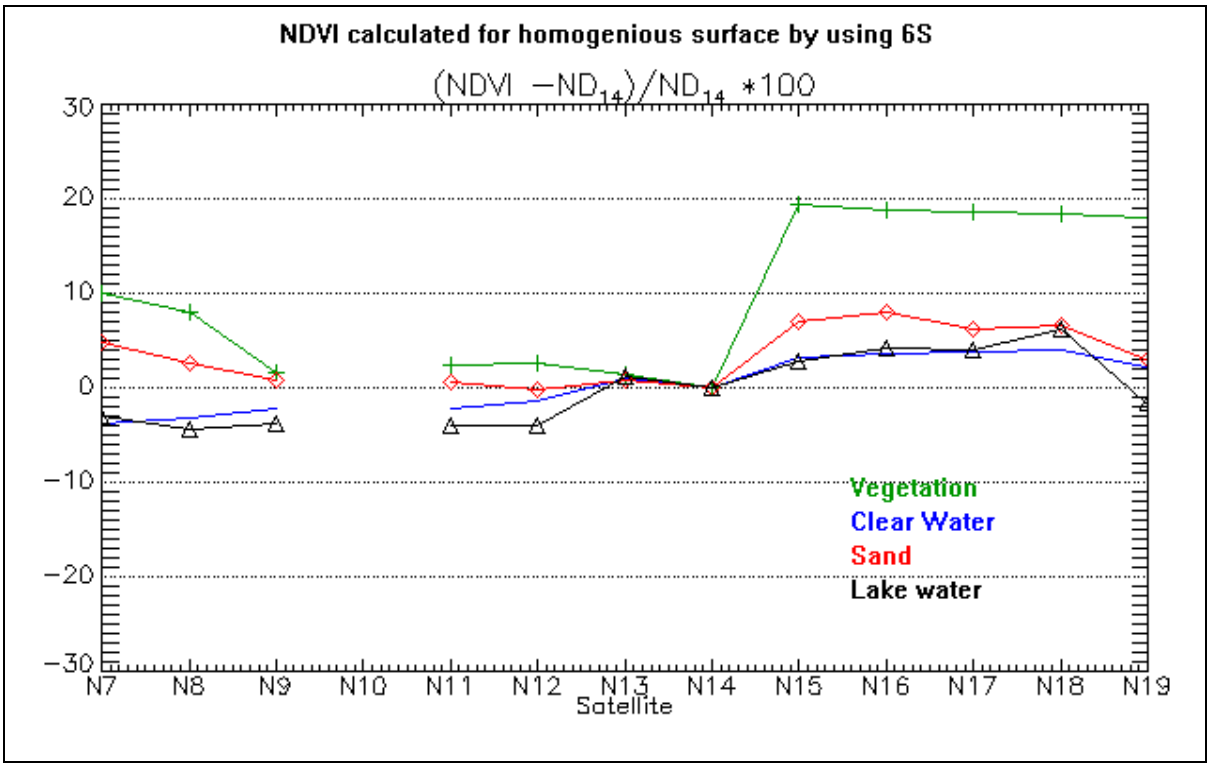

Figure 11. NDVI values calculated by 6S model from various NOAA satellites.

3.6 Practical Considerations

3.6.1 Numerical Computation Considerations

The whole algorithm is composed of many straight forward calculations, thus, it is light computationally.

3.6.2 Programming and Procedural Considerations

VHP code is run every day with all the available AVHRR GAC input data for making the daily composites. It also runs once per week to make weekly MVC composites and produce the vegetation health indices.

3.6.3 Quality Assessment and Diagnostics

Unit testing and system testing will include quality assessment with historical in situ observations.

3.6.4 Exception Handling

The expected exceptions, and a description of how they are identified, trapped, and handled, will be provided in a future version of this document.

3.7 Sample Results

Figure 12 shows examples of composite maps presenting typical summer and winter Vegetation Health maps produced by this algorithm. Left column is for week 26 (June 2009), and right column is for week 52 (December 2009). Vegetation Health is unit-less.
The retrieved Vegetation Health values generally exhibit a good dynamic range from 0-100 indicating that this algorithm is capable of retrieving the required range of Vegetation Health values given different vegetation type and brightness temperature inputs from satellite sensors. The spatial patterns shown in the maps are also consistent with global dry/wet patterns of climate regimes.

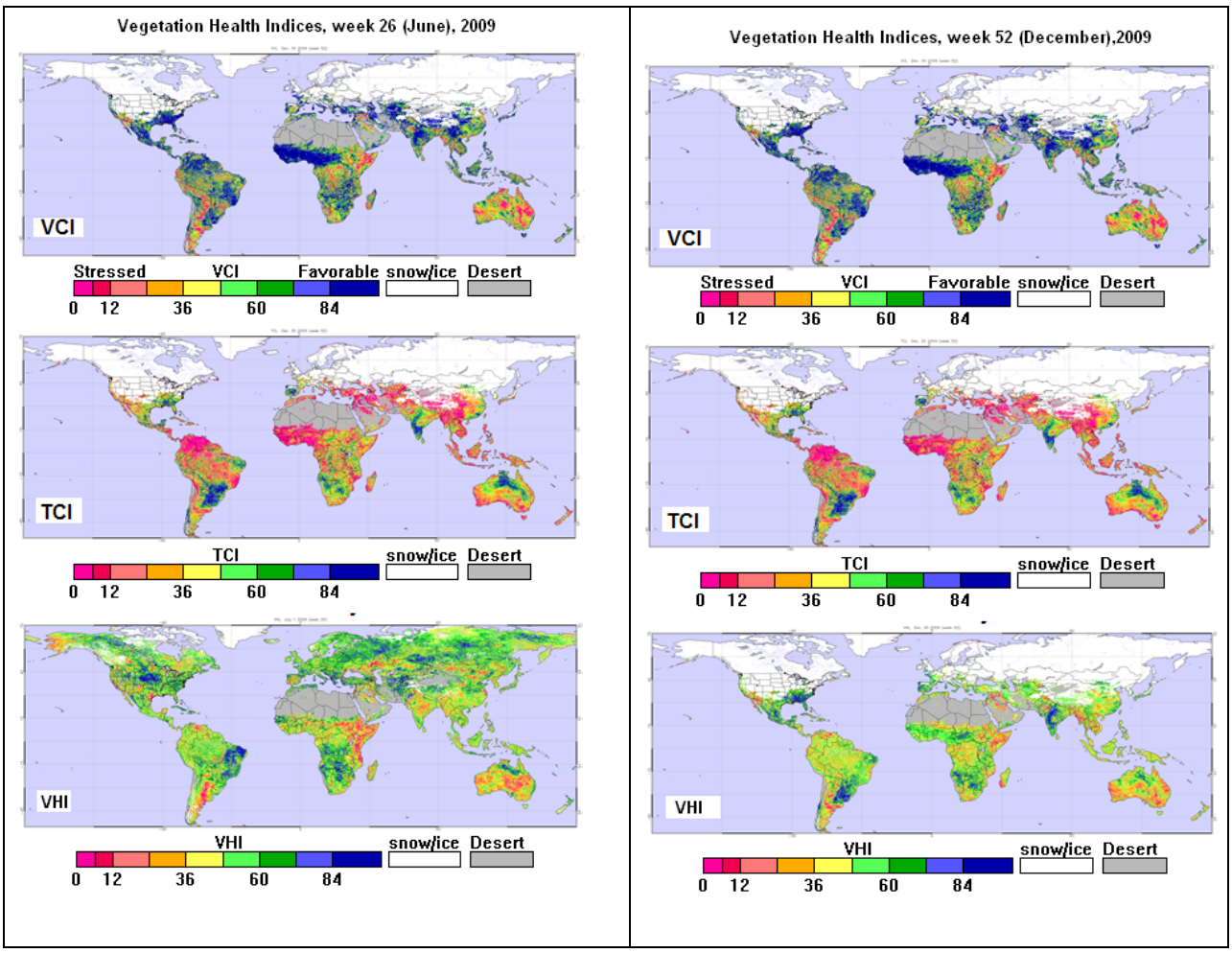

Figure 12. Vegetation Health maps produced by the VHP algorithm (left): Summer, week 26 - June 2009, (right) winter, week 52 - December 2009.

3.8 Validation Efforts

3.8.1 Validation of VPH algorithm with science data

In the efforts to quantitatively assess the VHP algorithm, similar products from other satellites or from other developing teams were compared.

Figures 13, 14 and 15 show NDVI time series from GVPS, GIMMS and MODIS data sets.

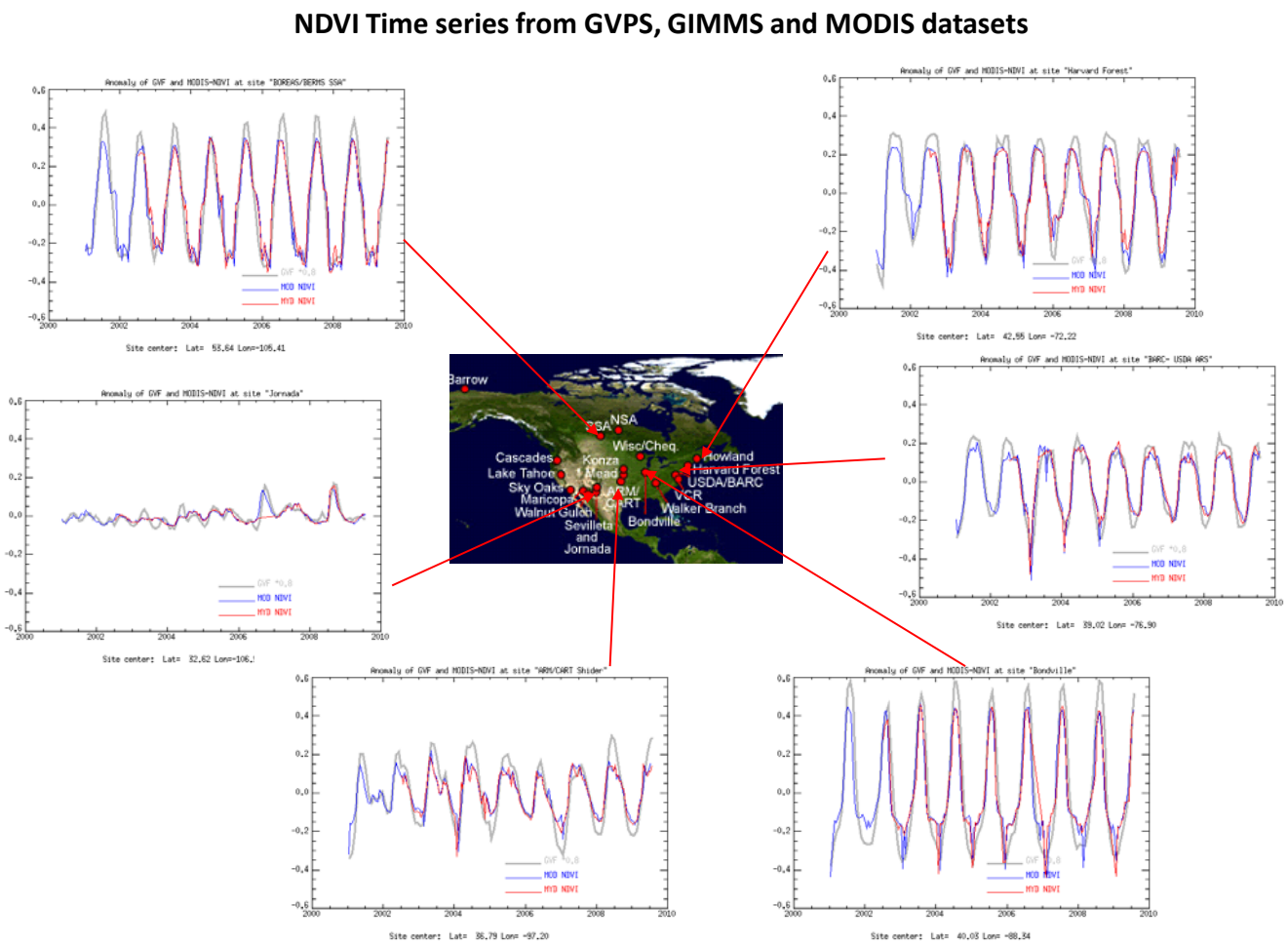

Figure 13. NDVI time series from GVPS, GIMMS and MODIS data sets.

NDVI Anomaly

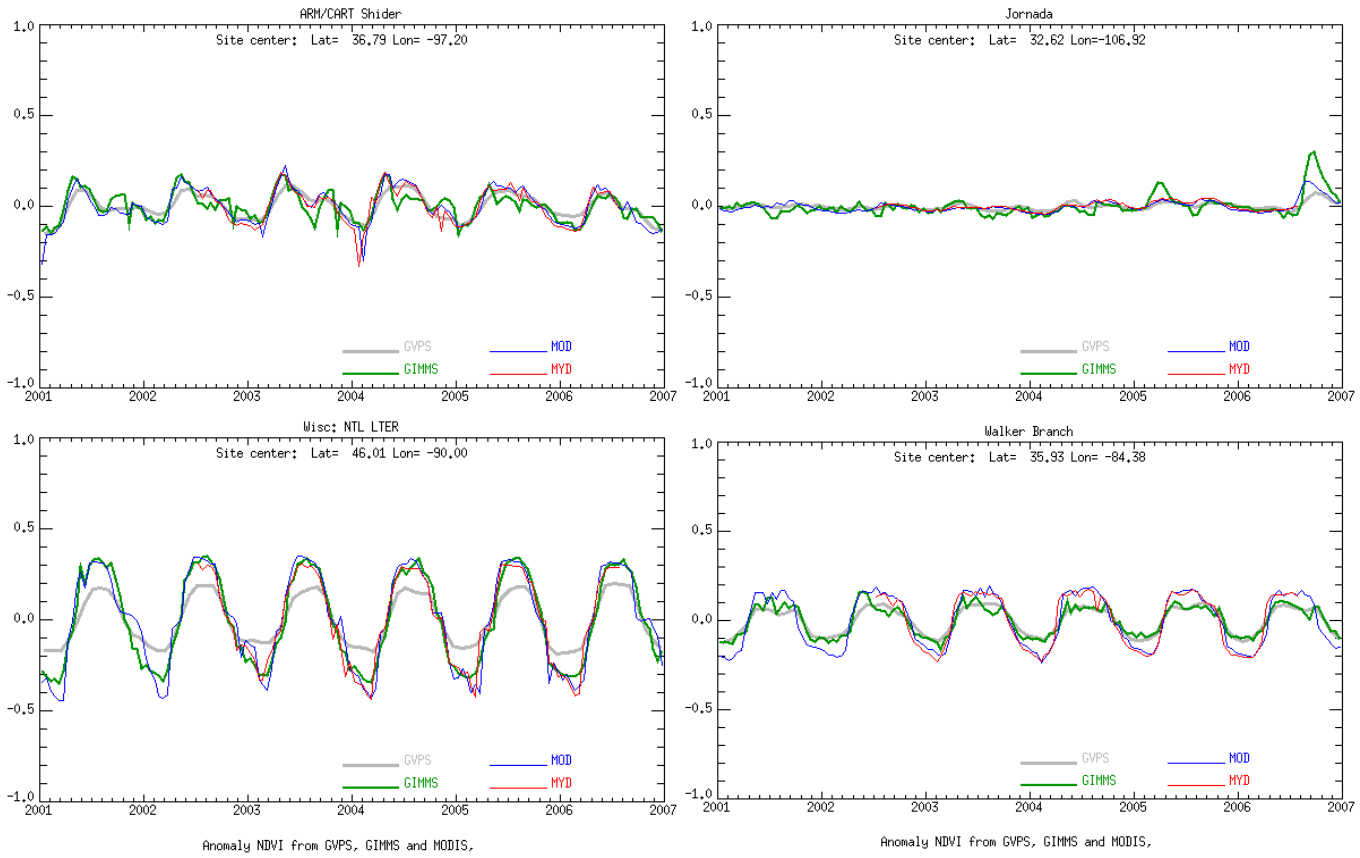

Figure 14. Time series of NDVI from AVHRR retrievals and NDVI from MODIS.

"Normalized" NDVI Time Series from GVPS, GIMSS and MODIS data sets.

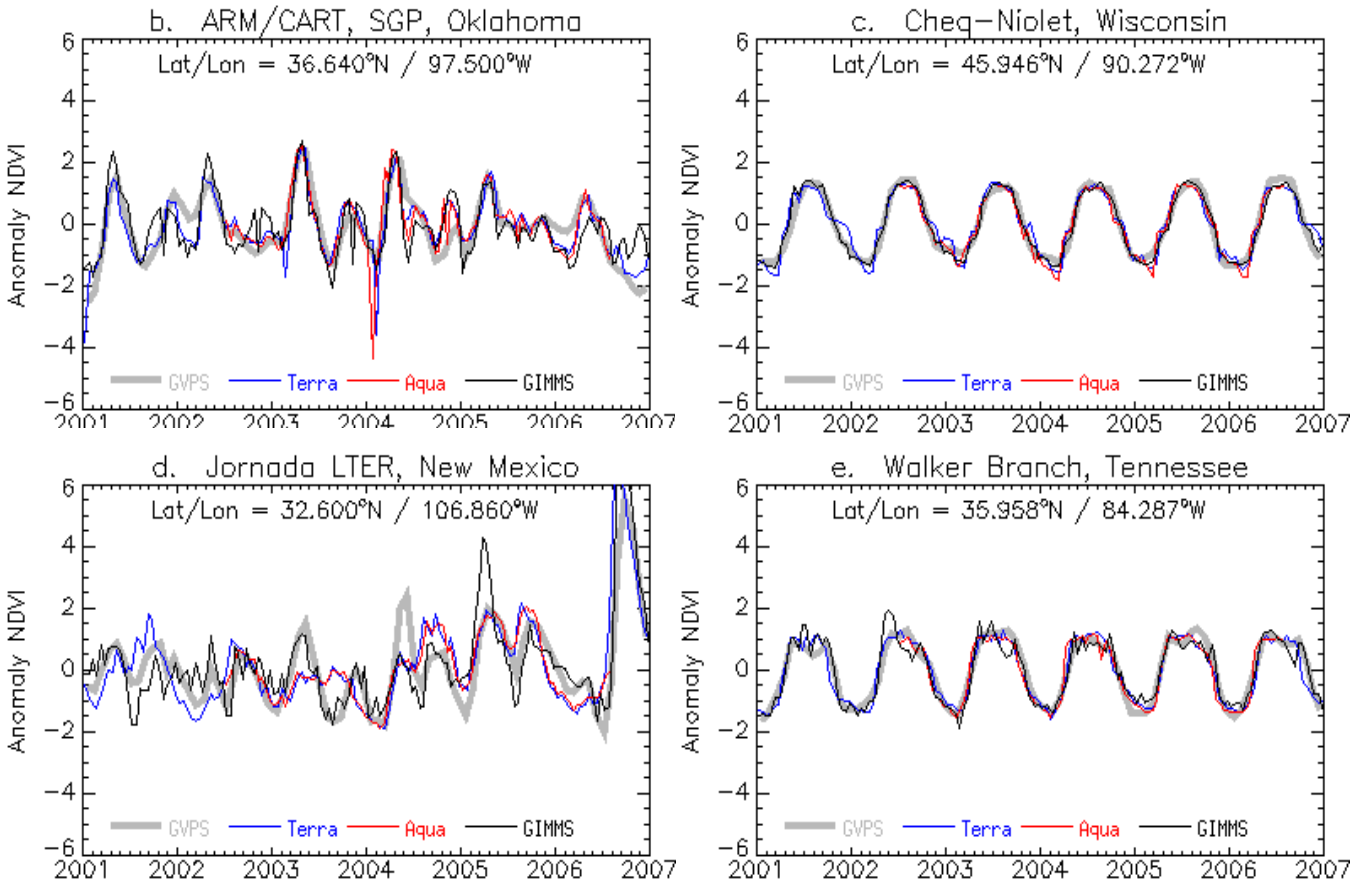

Figure 15. Time series of NDVI from AVHRR retrievals and NDVI from MODIS.

The results presented above show that time series (NDVI) from the VHP algorithm are consistent with time series from other sensors and developing teams.

4. ASSUMPTIONS AND LIMITATIONS

4.1 Assumptions

The assumptions that were made in producing Vegetation Health product using VHP include:

- NDVI change is slow and smooth from week to week. Abnormal jumps in NDVI time series will be considered as noise and be removed.
- The time latency of the VHP products is within 6 hours after the end of each 7-day period.

4.2 Limitations

- The VHP will not retrieve Vegetation Health in snow and desert areas.
- The VHP system will produce vegetation health indices for the “global” area from 55º S to 75º N

5. RISKS AND RISK REDUCTION EFFORTS

5.1 Failure of AVHRR Sensor on NOAA series satellite.

The AVHRR sensor on NOAA series satellites has been in space since September 1981. VHP uses AVHRR observations from afternoon satellites as the primary data input and its success has a risk of AVHRR failure. However, it is possible to produce similar products from MetOp satellites which are morning orbital satellites. MetOp is a series of polar orbiting meteorological satellites operated by the European Organization for the Exploitation of Meteorological Satellites (EUMETSAT). AVHRR on MetOp satellites also have higher spatial resolution (1km). By properly scaling, the VHP products from both data sources can be merged into one comprehensive product.

5.2 AVHRR Unavailability

If input AVHRR data from both NOAA series satellites and MetOp satellites are unavailable, The VHP may be produced from Moderate-resolution Imaging Spectroradiometer (MODIS), Visible Infrared Imager Radiometer Suite (VIIRS), Spinning Enhanced Visible and Infrared Imager (SEVIRI) and/or Advanced Baseline Imager (ABI) sensors. MODIS and VIIRS are onboard polar satellites with higher spatial resolution (250m at nadir). SEVIRI and ABI are onboard geostationary satellites with higher observing frequency (for example, SEVIRI has 3km resolution at nadir with 15 minutes interval). The converting algorithm is still under investigation.

6. LIST OF REFERENCES

Cracknell, A.P. 1997: The Advanced Very High resolution Radiometer. Taylor & Francis, USA, 534 p.

Crosby, D. S., Goldberg M. D. and W. Chung 1996, Inter-satellite calibration using empirical distribution functions. *8th Conference on Satellite Meteorology and Ocean, Atlanta GA. American. Meteorological Society*, 188-190.

Heidinger, Andrew K. and Pavolonis, Michael J. Global daytime distribution of overlapping cirrus cloud from NOAA's Advanced Very High Resolution Radiometer. Journal of Climate, Volume 18, Issue 22, 2005, pp.4772-4784.

Jacobowitz, H., Stow, L.L., Ohring, G., Heidinger, A., Knapp, K. and Nalli, N. 2003: The Advanced Very High Resolution Radiometer PATHFINDER Atmosphere (PATMOS) climate data set: A Resource for Climate Research. *Bull. American Meteorological Society,* June, 785-793.

James, M.E. and Kalluri, S.N., 1994: The Pathfinder AVHRR land data set: An improved coarse resolution data set for terrestrial monitoring. *Int. J. Remote Sensing* 15**,** 3347-3363.

Kidwell, K. B. (Ed), 1997, Global Vegetation Index User's Guide. National Oceanic and Atmospheric Administration, National Environmental Satellite Data and Information Services, National Climatic Data Center. Camp Springs MD, USA.

Kidwell, K. B. (Ed), 1995, NOAA Polar Orbiter Data Users Guide. National Oceanic and Atmospheric Administration, National Environmental Satellite Data and Information Services, National Climatic Data Center. Camp Springs MD, USA.

Kogan, F.N., 1997, Global Drought Watch from Space. *Bull. American Meteorological Society,* 78, 621-636.

Kogan, F. N. Sullivan, J.T. and Pu Bu Ciren, 1996. Testing post-launch calibration for the AVHRR sensor on world desert targets during 1985-1993. *Adv. Space Res., vol 17*, No 1, 47-50.

Kogan, F.N., 1995: Droughts of the Late 1980s in the United States as Derived from NOAA Polar Orbiting Satellite Data. *Bull. Amer. Meteor. Soc*. 76, 655-668.

Kogan, F.N., J. Sullivan, R. Carey and D.Tarpley, 1994: Post-Pinatubo Vegetation Index in Central Africa. *Geocarto International,* 3: 51-58

Liu, W.T. and F. Kogan (2002), Monitoring Brazilian soybean production using NOAA/AVHRR based vegetation condition indices. Int. J. Remote Sens., 23(6), 1161–1179.

Rao, C. R. N. and Chen, J., 1993, Calibration of the visible and near-infrared channels of the Advanced Very High Resolution Radiometer (AVHRR) after launch. Proceedings the Int. Soc. Optical Eng., Orlando, Florida, 56-66.

Rao, C. R. N. and Chen, J., 1999, Revised post-launch calibration of the visible and near-infrared channels of the Advanced Very High Resolution Radiometer on the NOAA-14 spacecraft. *Int. J. of Remote Sensing*, 20, pp. 3485.Salazar, L., Kogan, F. and L. Roytman (2007), Use of remote sensing data for estimation of winter wheat yield in the United States. Int. J. Remote Sens., 28(17), 3795-3811.

Tarpley, J.P., Schneider, S.R. and Money, R.L. 1984: Global vegetation index from NOAA-7 meteorological satellite. *J. Climate & Applied Meteorology*, 23, 491-494.

Vargas, M., Kogan, F and Guo, W. 2009: Empirical normalization for the effect of volcanic stratospheric aerosols on AVHRR NDVI. *Geophysical Research Letters, vol 36*.

Tucker, C.J., Pinzon, J.E., Brown, M.B., Slayback, D.A., Pak, E.W., Mahoney, R., Vermote, E.F. and El Salcous, N. 2004: An extanded AVHRR 8-km NDVI data set compatible with MODIS and SPOT vegetation NDVI data. *Int. J. Remote Sensing*.

END OF DOCUMENT